

Conformation of K^+ (Crown Ether) Complexes Revealed by Ion Mobility–Mass Spectrometry and Ultraviolet Spectroscopy

Sota Tainaka, Tomoyuki Ujihira, Mayuko Kubo, Motoki Kida, Daisuke Shimoyama, Satoru Muramatsu, Manabu Abe, Takeharu Haino, Takayuki Ebata, Fuminori Misaizu, Keijiro Ohshimo,* and Yoshiya Inokuchi*

Cite This: <https://dx.doi.org/10.1021/acs.jpca.0c09068>

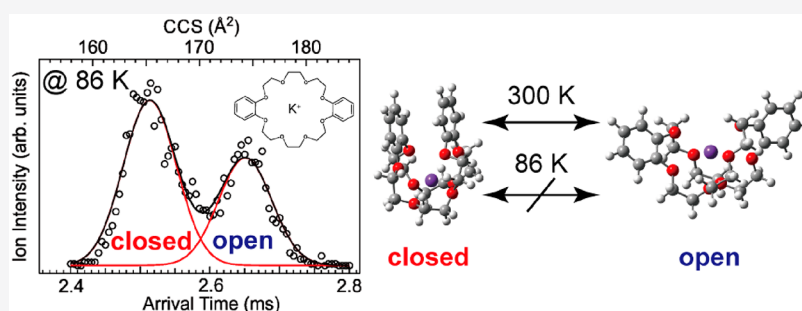
Read Online

ACCESS |

Metrics & More

Article Recommendations

Supporting Information



ABSTRACT: The conformation and electronic structure of dibenzo-24-crown-8 (DB24C8) complexes with K^+ ion were examined by ion mobility–mass spectrometry (IM–MS), ultraviolet (UV) photodissociation (UVPD) spectroscopy in the gas phase, and fluorescence spectroscopy in solution. Three structural isomers of DB24C8 (SymDB24C8, Asym1DB24C8, and Asym2DB24C8) in which the relative positions of the two benzene rings were different from each other were investigated. The IM–MS results at 86 K revealed a clear separation of two sets of conformers for the K^+ (SymDB24C8) and K^+ (Asym1DB24C8) complexes whereas the K^+ (Asym2DB24C8) complex revealed only one set. The two sets of conformers were attributed to the open and closed forms in which the benzene–benzene distances in the complexes were long (>6 Å) and short (<6 Å), respectively. IM–MS at 300 K could not separate the two conformer sets of the K^+ (SymDB24C8) complex because the interconversion between the open and closed conformations occurred at 300 K and not at 86 K. The crown cavity of DB24C8 was wrapped around the K^+ ion in the complex, although the IM–MS results availed direct evidence of rapid cavity deformation and the reconstruction of stable conformers at 300 K. The UVPD spectra of the K^+ (SymDB24C8) and K^+ (Asym1DB24C8) complexes at ~ 10 K displayed broad features that were accompanied by a few sharp vibronic bands, which were attributable to the coexistence of multiple conformers. The fluorescence spectra obtained in a methanol solution suggested that the intramolecular excimer was formed only in K^+ (SymDB24C8) among the three complexes because only SymDB24C8 could possibly assume a parallel configuration between the two benzene rings upon K^+ encapsulation. The encapsulation methods for K^+ ion (the “wraparound” arrangement) are similar in the three structural isomers of DB24C8, although the difference in the relative positions of the two benzene rings affected the overall cross-section. This study demonstrated that temperature-controlled IM–MS coupled with the introduction of appropriate bulky groups, such as aromatic rings to host molecules, could reveal the dynamic aspects of encapsulation in host–guest systems.

INTRODUCTION

Crown ethers are widely employed as host molecules or building blocks of supramolecular systems. One of the characteristic functions of crown ethers is ion selectivity.^{1,2} The most famous combination of crown ethers with metal ion guests is that between 18-crown-6 (18C6) and K^+ . It has been suggested that an optimum size matching of 18C6 with a K^+ ion could result in K^+ ion selectivity of 18C6 among the alkali metal ions and that the conformation of the crown part could be key to effective encapsulation. The encapsulation structures of crown ether complexes have been mainly investigated in crystal forms by X-ray diffraction (XRD).^{3–6} However, it is

challenging to apply XRD to all of the complexes because it requires the crystallization of the complexes. Another method of determining the structure of crown ether complexes is ion mobility–mass spectrometry (IM–MS) in the gas phase.^{7–24} Most previous IM–MS studies were focused on elucidating the

Received: October 6, 2020

Revised: November 9, 2020

conformations of biomolecular ions. Regarding IM–MS of host–guest or supramolecular systems, Bowers and coworkers reported experiments on 18C6 complexes with alkali metal ions.²⁵ The arrival time distribution (ATD) of the $K^+(18C6)$ complex revealed one component, which indicated the presence of a single structure or a set of very similar structures.²⁵ The capacity of IM–MS to distinguish different conformations for host–guest systems has not been demonstrated. Dearden and coworkers also reported the MS–MS studies on host–guest complexes.^{26,27} More recently, crown ether complexes with metal ions were investigated in the gas phase through spectroscopic techniques.^{28–39} Ultraviolet photodissociation (UVPD) spectroscopy performed under cold, gas-phase conditions could highly distinguish several conformers.^{28,29,37–42} However, the UVPD spectra of larger systems tend to reveal broad spectral features, which limited the distinction of different conformers or the determination of their structures.⁴³ Rizzo and coworkers reported pioneering works on the cold-ion spectroscopy of biomolecular ions selected by IM.^{44,45} They elaborated on the relation between the conformation and spectroscopic features.

In this study, we investigated the conformation of K^+ complexes with three structural isomers of dibenzo-24-crown-8 (DB24C8) by IM–MS and UVPD spectroscopy in the gas phase. Figure 1 shows the structural isomers

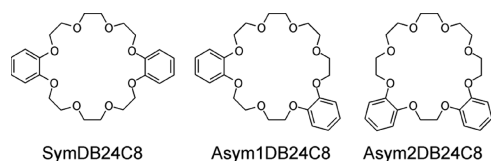


Figure 1. Structural isomers of DB24C8 (SymDB24C8, Asym1DB24C8, and Asym2DB24C8).

(SymDB24C8, Asym1DB24C8, and Asym2DB24C8) of the studied DB24C8. In these isomers, the relative positions of the benzene rings were different. We have previously reported that the $K^+(\text{SymDB24C8})$ complex exhibited broad UV absorption even under cold, gas-phase conditions, and this was attributable to the formation of an intramolecular excimer upon irradiation by UV light.⁴³ Conversely, the $K^+(\text{SymDB24C8})$ complex has been suspected to exhibit another type of conformation because weak, sharp bands also appeared from the broad absorption.⁴³ However, these sharp bands were too weak to be identified as different conformers through double-resonance spectroscopies.^{28,29,39–42} The IM–MS experiment is free from the restriction originating from the optical transition such as the oscillator strength, and it can separate different conformers and determine the abundance ratio quantitatively. Here, we examined (1) the capacity of

IM–MS to separately detect the conformers and (2) the effect of the difference in the relative positions of the benzene rings on the electronic and geometric structures of the $K^+(\text{DB24C8})$ complexes.

EXPERIMENTAL AND COMPUTATIONAL METHODS

UVPD Spectroscopy in the Gas Phase and Fluorescence Spectroscopy in Solution. The experimental details of UVPD spectroscopy, which was performed at Hiroshima University, were presented in our previous papers.^{39,41} Briefly, the $K^+(\text{SymDB24C8})$, $K^+(\text{Asym1DB24C8})$, and $K^+(\text{Asym2DB24C8})$ complexes were produced from an electrospray ionization (ESI) ion source utilizing methanol solutions of KCl and SymDB24C8, Asym1DB24C8, or Asym2DB24C8 ($\sim 100 \mu\text{M}$ each). The complexes were introduced into a cold, Paul-type quadrupole ion trap (QIT). QIT was cooled to $\sim 4 \text{ K}$ by a He cryostat with a continuous flow of He buffer gas. The ions were stored in QIT for $\sim 90 \text{ ms}$ to be translationally and internally cooled by collision with the cold He buffer gas. The vibrational temperature of the trapped ions was estimated to be $\sim 10 \text{ K}$.³⁹ The ions other than the parent ones of interest were removed from QIT by applying a radio frequency (RF) potential to the entrance end-cap.⁴⁶ The cold complexes were irradiated afterward by a UV radiation. The resulting fragment ions were mass-analyzed and detected with a home-made time-of-flight (TOF) mass spectrometer.⁴⁷ The UVPD spectra of the $K^+(\text{SymDB24C8})$, $K^+(\text{Asym1DB24C8})$, and $K^+(\text{Asym2DB24C8})$ complexes were obtained by plotting the yields of the fragment K^+ ions against the wavenumber of the UV laser. The UV laser was obtained by the second-harmonic generation employing the fundamental output of a dye laser (Continuum ND6000) pumped with the third harmonic of an Nd^{3+} :YAG laser (Continuum Surelite II). The fluorescence spectra of SymDB24C8, Asym1DB24C8, and Asym2DB24C8 dissolved in methanol with/without KCl salt were observed at $\sim 300 \text{ K}$ utilizing a commercial fluorescence spectrometer (HORIBA Fluoromax-4).

Ion Mobility–Mass Spectrometry (IM–MS). The present IM experiments were performed with a home-made IM mass spectrometer at Tohoku University (Figure 2).²⁴ The apparatus consisted of four chambers that were separately pumped to vacuum. The following components were placed in each chamber: (i) an ESI ion source, (ii) QIT and an ion–drift cell with an ion funnel, (iii) an octopole ion guide and acceleration electrodes for TOF–MS, and (iv) reflection electrodes and a microchannel plate (MCP) for ion detection.

Each of the three DB24C8 structural isomers and KCl salt were dissolved in methanol to prepare solutions with

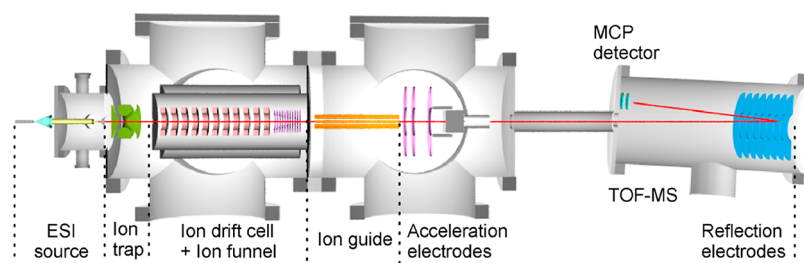


Figure 2. Schematic of the IM mass spectrometer at Tohoku University.

concentrations of $\sim 100 \mu\text{M}$ each. The solution was loaded into a metal capillary by a syringe pump at $1 \mu\text{L}/\text{min}$, after which high voltage ($+3.3 \text{ kV}$) was applied to the capillary. The exit of the capillary was positioned $\sim 5 \text{ mm}$ from the entrance of a heated desolvation capillary that was maintained at $\sim 320 \text{ K}$. The exit of the desolvation capillary was inserted into the first vacuum chamber whose pressure was 0.25 Torr . The first chamber was connected to the second chamber via a conical skimmer.

After passing through the skimmer, the ions were introduced into QIT (Jordan TOF Products, C-1251) in the second chamber. The ions accumulated for 90 ms in the ion trap. Afterward, the ions were injected into the ion drift cell by a pulsed electric field with a kinetic energy of 10 eV in the laboratory frame at a given time ($t = t_0$). The repetition rate of ion injection was 10 Hz . The total drift length from the entrance to exit apertures of the cell was 327 mm . The diameters of the two apertures were 2.0 mm each. In the cell, a static electric field, $E = 4.6 \text{ V}/\text{cm}$, was applied for ion drifting. To collect the ions, the ion funnel was attached to the end of the cell.⁴⁸ Additionally, a cryogenic jacket surrounding the ion–drift cell was filled with liquid nitrogen. A similar cryogenic jacket design was reported by May and Russell.⁴⁹ In these experiments, the temperature of the He buffer gas was 86 K , and its pressure was maintained at 0.49 Torr through a variable leak valve. Therefore, the E/N value was 8.3 Td (N is the number density of the buffer gas, $1 \text{ Td} = 10^{-17} \text{ V cm}^2$). The pressures in the second and third chambers were 1×10^{-4} and $6 \times 10^{-5} \text{ Torr}$, respectively.

After passing through the ion–drift cell, the ions were transported through the octopole ion guide to the acceleration region of the TOF mass spectrometer. The ions were reaccelerated at a kinetic energy of $\sim 1.4 \text{ keV}$ into the reflectron TOF mass spectrometer by applying the pulsed electric field to the acceleration electrodes at a given time later (Δt) from the pulse for the injection into the drift cell (t_0), namely $t = t_0 + \Delta t$. This delay time between the two pulses, Δt , is defined as the “arrival time”, and it was controlled by a digital delay/pulse generator. This arrival time consisted of the drift times in three regions: (i) the region between the center of QIT and the entrance of the cell, (ii) the one inside the cell, and (iii) that between the exit of the cell and the acceleration region of the TOF mass spectrometer. To evaluate the drift velocity of the cell to satisfy the measured arrival time, we calculated the drift time in the three regions by solving the equations of the motion of the ions. Therefore, we obtained the time spent by an ion in the cell from the measured arrival time. The drift time in the cell depends on the collision cross sections (CCSs) between the ions and He atoms. Ions with different CCSs arrived at the acceleration region of the spectrometer at different times. Finally, the ions were mass-analyzed by a reflectron TOF mass spectrometer. The pressure in the chamber of the TOF spectrometer was $1 \times 10^{-6} \text{ Torr}$. During IM–MS measurement, we obtained a series of TOF mass spectra sequentially by scanning the arrival times. Resultantly, the ions with different CCSs were separately detected at different arrival times in a two-dimensional plot of TOF versus arrival time. We obtained ATD by plotting the ion intensity of a given TOF peak against a function of the arrival time. The mobility resolution of the apparatus, which was estimated from ATD of Li^+ ion-encapsulated fullerene ($\text{Li}^+@C_{60}$) with a single isomer, was ~ 30 .⁵⁰

Computational Methods. Further, we conducted quantum chemical calculations on the $\text{K}^+(\text{SymDB24C8})$, $\text{K}^+(\text{Asym1DB24C8})$, and $\text{K}^+(\text{Asym2DB24C8})$ complexes. The initial conformational search was performed by the CONFLEX High-Performance Conformation Analysis program with an MMFF94s force field.^{51–54} The structures obtained by the initial search were further optimized by the Gaussian 09 program package at the M05-2X/6-311++G(d,p) level of theory.⁵⁵ The vibrational analysis was also performed at the same calculation level.

The collision integrals of the complex ions with a He atom were calculated by the trajectory method that is included in the MOBCAL program.⁵⁶ When an ion and a He atom were considered as hard spheres without internal states, the collision integral was reduced to the hard-sphere CCS. In the trajectory method, the interaction potential between the ion and a He atom was required. This interaction potential comprised the sum of the interaction potentials between the constituent atoms of the complexes (H, C, O, K atoms) and a He atom, $V_i^{\text{X-He}}(r_i)$, as shown in eq 1:

$$V_i^{\text{X-He}}(r_i) = 4e^{\text{X-He}} \left[\left(\frac{\sigma^{\text{X-He}}}{r_i} \right)^{12} - \left(\frac{\sigma^{\text{X-He}}}{r_i} \right)^6 \right] - \frac{\alpha e^2 q_i^2}{2 r_i^4} \quad (\text{X} = \text{H, C, O, K}) \quad (1)$$

where r_i is the distance between the i th constituent atom and a He atom, $\epsilon^{\text{X-He}}$ and $\sigma^{\text{X-He}}$ are the Lennard–Jones parameters, α is the polarizability of a He atom, and q_i is the partial atomic charge on the constituent atoms. On the right side of the equation, the first term represents the Lennard–Jones potential between neutrals and the second represents the charge–induced dipole interaction between q_i and a He atom. Here, we adopted the values determined in the previous study for $\epsilon^{\text{X-He}}$ and $\sigma^{\text{X-He}}$ ($\text{X} = \text{H, C, O}$).⁵⁷ For $\epsilon^{\text{K-He}}$, we adopted the interaction energy of the K–He complex of the optimized structure. Additionally, we adopted the bond distance in the K^+ –He complex for $\sigma^{\text{K-He}}$ assuming that the partial atomic charge of the K atom is $+1$. The CCSD(T)/6-311+G(d,p) level was employed for the calculations of K–He and K^+ –He. The values of $\epsilon^{\text{X-He}}$ and $\sigma^{\text{X-He}}$ adopted here are summarized in Table 1. The partial atomic charges, q_i , were calculated by natural population analysis. Furthermore, 86 K was adopted as the temperature value in the trajectory calculations.

Table 1. Values of $\epsilon^{\text{X-He}}$ and $\sigma^{\text{X-He}}$ Adopted in This Study

X	$\epsilon^{\text{X-He}}/\text{meV}$	$\sigma^{\text{X-He}}/\text{\AA}$
H	0.6175	2.2610
C	1.3266	3.0126
O	1.0720	2.4344
K	0.5151	2.6368

Chemicals. Commercially available SymDB24C8 was purchased and utilized without further purification. Asym1DB24C8⁵⁸ and Asym2DB24C8⁵⁸ were synthesized by previously reported modified procedures. All of the reagents and solvents were of commercial reagent grade and were utilized without further purification except otherwise noted. Dry DMF and DMSO were obtained by distillation over CaH_2 . The ^1H and ^{13}C NMR spectra were recorded on a Varian mercury-300 spectrometer (operating at 300 and 75 MHz for

^1H and ^{13}C NMRs, respectively) employing CDCl_3 as the solvent. All of the spectra were recorded at 298 K, and the chemical shifts were reported on the delta scale in ppm relative to CHCl_3 ($\delta = 7.26$ for ^1H and 77.2 for ^{13}C). The infrared (IR) spectra were recorded on a HORIBA FT-720 spectrometer. Preparative separations were performed by silica gel gravity column chromatography (silica gel 60 N (spherical, neutral)). Recycling preparative gel permeation chromatography (GPC)–high-performance liquid chromatography (HPLC) (GPC–HPLC) separations were performed on JAI LC-908s employing preparative JAIGEL-2H, 2H, and 1H columns in series. High-resolution MS (HRMS) was performed on a Thermo Fisher Scientific LTQ Orbitrap XL spectrophotometer, and the spectra were obtained by ESI method.

Synthesis of 6,7,9,10,12,13,15,16,23,24,26,27-Dodecahydrodibenzo[B,k][1,4,7,10,13,16,19,22]-octaoxacyclotetracosine (a). A mixture of bis[2-(*o*-hydroxyphenoxy)ethyl]ether (0.950 g, 3.27 mmol) and K_2CO_3 (1.06 g, 7.67 mmol) in DMSO (8.95 mL) was stirred with heating at 363 K. To the mixture was added bis(*p*-toluenesulfonyl) tetraethylene glycol (0.895 g, 1.78 mmol) in DMF (8.95 mL) within 3 h. After heating for 5 d, the reaction mixture was acidified to pH 5–6 with HCl and extracted with CH_2Cl_2 . The organic layer was dried over Na_2SO_4 , and the solvent was removed in vacuo. The crude product was purified by column chromatography with alumina as the adsorbent (hexane/ethyl acetate) to yield Asym1DB24C8 as a colorless oil (0.490 g, 33%).

^1H NMR (300 MHz, CDCl_3): δ 6.91 (m, 8H), 4.20 (t, 4H, $J = 5.0$ Hz), 4.15 (t, 4H, $J = 3.7$ Hz), 4.00 (t, 4H, $J = 5.0$ Hz), 3.88 (t, 4H, $J = 3.7$ Hz), 3.78 (m, 4H), and 3.70 (m, 4H) ppm; ^{13}C NMR (75 MHz, CDCl_3): δ 149.3, 148.9, 121.9, 121.5, 115.6, 114.2, 71.1, 70.7, 70.3, 69.8, 69.6, and 69.1 ppm; Fourier-transform IR (FT–IR)–attenuated total reflection (ATR) (neat): ν 2929, 1594, 1506, 1254, and 930 cm^{-1} ; HRMS (ESI–Orbitrap): calcd for $\text{C}_{24}\text{H}_{32}\text{O}_8\text{Na}$ m/z 471.1989 $[\text{M} + \text{Na}]^+$, found m/z 471.1982.

Synthesis of 6,7,9,10,12,13,15,16,18,19,26,27-Dodecahydrodibenzo[B,h][1,4,7,10,13,16,19,22]-octaoxacyclotetracosine (b). A mixture of 1,2-bis(*o*-hydroxyphenoxy)ethane (0.0925 g, 0.375 mmol) and K_2CO_3 (0.103 g, 0.745 mmol) in DMF (1.84 mL) was stirred with heating at 363 K. To the mixture was added bis(*p*-toluenesulfonyl) pentaethylene glycol (0.207 g, 0.377 mmol) in DMF (1.84 mL) within 3 h, and the mixture was heated for 3 d. The mixture was acidified to pH 5–6 with HCl and extracted with CH_2Cl_2 . The organic layer was dried over Na_2SO_4 , and the solvent was removed in vacuo. The crude product was purified by a recycling preparative GPC–HPLC system to yield Asym2DB24C8 as a colorless oil (0.0500 g, 30%).

^1H NMR (300 MHz, CDCl_3): δ 6.94 (m, 8H), 4.38 (s, 4H), 4.18 (t, 4H, $J = 4.7$ Hz), 3.85 (t, 4H, $J = 4.7$ Hz), 3.72 (m, 4H), and 3.62 (m, 8H) ppm; ^{13}C NMR (75 MHz, CDCl_3): δ 149.5, 149.1, 122.2, 121.8, 116.2, 115.3, 71.1, 70.9, 70.9, 69.9, 69.4, and 68.7 ppm; FT–IR–ATR (neat): ν 2870, 1592, 1497, 1253, 1113, and 930 cm^{-1} ; HRMS (ESI–Orbitrap): calcd for $\text{C}_{24}\text{H}_{32}\text{O}_8\text{Na}$ m/z 471.1989 $[\text{M} + \text{Na}]^+$, found m/z 471.1988.

RESULTS AND DISCUSSION

UVPD Spectra in the Gas Phase and Fluorescence Spectra in Solution. Figure 3 shows the UVPD spectra of

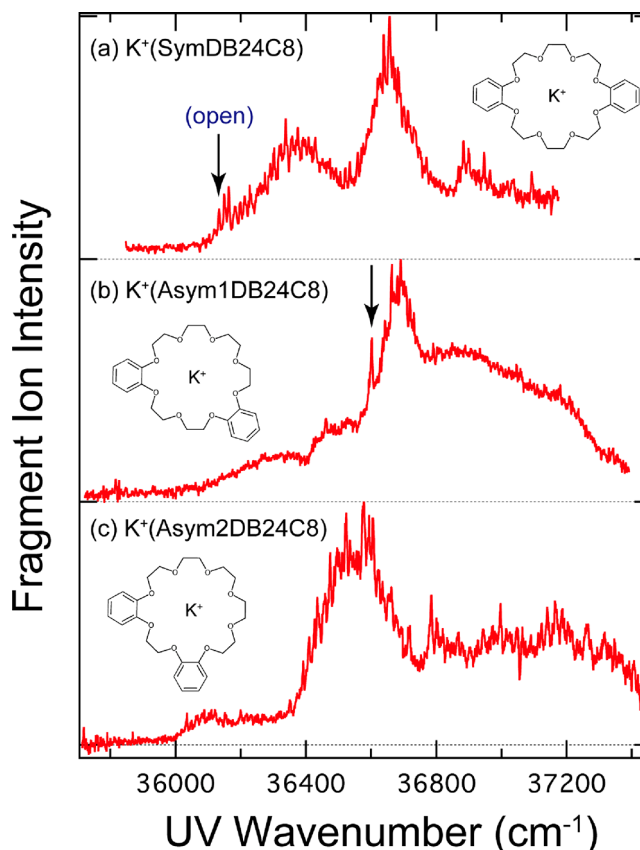


Figure 3. UVPD spectra of (a) $\text{K}^+(\text{SymDB24C8})$, (b) $\text{K}^+(\text{Asym1DB24C8})$, and (c) $\text{K}^+(\text{Asym2DB24C8})$. The spectrum of the $\text{K}^+(\text{SymDB24C8})$ complex was adopted from the previous study (ref 43, Copyright 2018 John Wiley and Sons). Sharp bands were also observed on the broad components (black arrows in panels a and b).

the DB24C8 complexes with K^+ ions observed under cold (~ 10 K) gas-phase conditions. The UVPD spectrum of the $\text{K}^+(\text{SymDB24C8})$ complex (Figure 3a), which was reproduced from our previous study,⁴³ was employed for comparison with those of the $\text{K}^+(\text{Asym1DB24C8})$ and $\text{K}^+(\text{Asym2DB24C8})$ complexes (Figure 3b,c). The $\text{K}^+(\text{SymDB24C8})$ complex exhibited a dominant conformer that displayed broad spectral features, which related to the formation of the intramolecular excimer.⁴³ Weak, sharp vibronic bands in addition to the broad features were also observed around 36 150 cm^{-1} (black arrow in Figure 3a). These bands were assigned to a minor conformer, indicating the coexistence of multiple conformers.⁴³ The UVPD spectrum of $\text{K}^+(\text{Asym1DB24C8})$ (Figure 3b) exhibited broad absorption in the 36 000–37 400 cm^{-1} region. Additionally, a few sharp bands were also detected on the broad component of the $\text{K}^+(\text{Asym1DB24C8})$ complex (one of the sharp bands is represented by an arrow at 36 603 cm^{-1} in Figure 3b). These spectral features also implied the coexistence of multiple conformers of $\text{K}^+(\text{Asym1DB24C8})$. Regarding the $\text{K}^+(\text{Asym2DB24C8})$ complex, the UVPD spectrum exhibited absorption in the 36 000–37 400 cm^{-1} region. Resolved vibronic structures could be observed around 36 500 cm^{-1} ,

although the spectrum was highly congested. It is difficult to apply double-resonance spectroscopic techniques to these complexes and determine the structure and number of their conformers, because the UV absorption of multiple conformers seems to be overlapped to each other.^{41,42}

Figure 4 shows the fluorescence spectra of SymDB24C8, Asym1DB24C8, and Asym2DB24C8 that were dissolved in

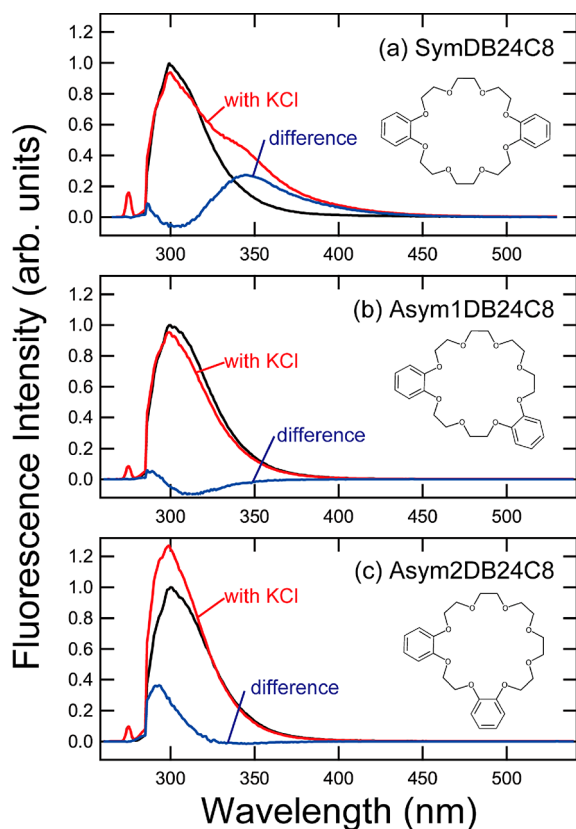


Figure 4. Fluorescence spectra of (a) SymDB24C8, (b) Asym1DB24C8, and (c) Asym2DB24C8 dissolved in methanol. The spectra of SymDB24C8 were adopted from the previous study (ref 43, Copyright 2018 John Wiley and Sons). The excitation wavelength was 275 nm.

methanol with/without KCl salt. The fluorescence spectra of SymDB24C8 (Figure 4a) were reproduced from the previous report for comparison.⁴³ The fluorescence spectrum of SymDB24C8 with KCl (red curve in Figure 4a) displayed a Stokes-shifted fluorescence peak at ~ 350 nm, and this was assigned to the intramolecular excimer of the $K^+(\text{SymDB24C8})$ complex formed upon UV irradiation.⁴³ The fluorescence spectra of Asym1DB24C8 and Asym2DB24C8 are displayed in Figure 4b,c. The difference spectra between the fluorescence spectra with/without KCl salt (blue curves in Figure 4b,c) exhibited maxima at ~ 287 and ~ 292 nm for Asym1DB24C8 and Asym2DB24C8, respectively, whereas the fluorescence spectra without KCl (black curves in Figure 4b,c) displayed a maximum at ~ 300 nm for both Asym1DB24C8 and Asym2DB24C8. These results indicated that the S_1-S_0 transitions of Asym1DB24C8 and Asym2DB24C8 slightly shifted to higher frequencies upon the formation of complexes with the K^+ ion. The blue-shift of the S_1-S_0 transition for the potassiated species was also observed for SymDB24C8.^{43,59} Neither the $K^+(\text{Asym1DB24C8})$ nor

$K^+(\text{Asym2DB24C8})$ complex showed Stokes-shifted excimer emissions that were observed in the $K^+(\text{SymDB24C8})$ complex. These fluorescence results indicated that the $K^+(\text{Asym1DB24C8})$ or $K^+(\text{Asym2DB24C8})$ complex did not form an intramolecular excimer in solution. Regarding SymDB24C8, the two benzene rings of the SymDB24C8 component drew close to each other upon the formation of a complex with the K^+ ion.⁴³ For Asym1DB24C8 and Asym2DB24C8, the relative positions of the benzene rings on the 24C8 component were unsuitable for the formation of the intramolecular excimer.

IM-MS Results. Figure 5 shows the ATDs of $K^+(\text{SymDB24C8})$, $K^+(\text{Asym1DB24C8})$, and $K^+(\text{Asym2DB24C8})$ observed at 86 K. Each ATD was fitted by Gaussian functions with a full width at half maximum (FWHM) of 90 μs . This width was determined from the mobility resolution of the apparatus, as aforementioned. Regarding $K^+(\text{SymDB24C8})$ and $K^+(\text{Asym1DB24C8})$ (Figure 5a,b), the ATD curves can be reproduced very well by two Gaussian functions, indicating the coexistence of two conformers or two sets of very similar conformers. The interval of the two Gaussian components was shorter for $K^+(\text{Asym1DB24C8})$ than for $K^+(\text{SymDB24C8})$. The ATD results in Figure 5a,b indicated that the interconversion between the two conformers did not occur in $K^+(\text{SymDB24C8})$ and $K^+(\text{Asym1DB24C8})$ at 86 K. In contrast, ATD of $K^+(\text{Asym2DB24C8})$ could be fitted by one Gaussian function. The experimental CCSs of the complexes were determined from the positions of the Gaussian components in the ATD data. The CCS values of the two group conformations were 165.3 (S-a) and 174.4 \AA^2 (S-b) for $K^+(\text{SymDB24C8})$ and 167.0 (AS1-a) and 173.5 \AA^2 (AS1-b) for $K^+(\text{Asym1DB24C8})$. The $K^+(\text{Asym2DB24C8})$ complex exhibited maximum distribution at 173.1 \AA^2 (AS2-a). The CCS values are listed in Table 2.

Geometric and Electronic Structures of the $K^+(\text{DB24C8})$ Complexes. We determined the conformation of the complexes by comparing the experimental and calculated CCS values. Figure 6 shows some representatives of the stable structures of $K^+(\text{DB24C8})$ obtained from the geometry optimization at the M05-2X/6-311++G(d,p) level. Further, we compared the stability of the stable conformers based on the relative Gibbs energy at 86 K (the same temperature as that of the IM-MS experiments). The conformations of the complexes were characterized by the distance between their benzene rings. Regarding the $K^+(\text{SymDB24C8})$ complex, the most stable structure (isomer **sym-a** (Figure 6a)) exhibited benzene-benzene distance of 3.82 \AA . The calculated CCS of this conformer was $163.5 \pm 0.6 \text{\AA}^2$. The second most stable structure (isomer **sym-b** (Figure 6b)) exhibited a longer benzene-benzene distance (9.33 \AA) than **sym-a**. This resulted in a larger CCS value ($172.8 \pm 0.8 \text{\AA}^2$) than that of **sym-a**. We named these isomers (**sym-a** and **sym-b**) closed and open conformers, respectively. The geometry optimization of $K^+(\text{Asym1DB24C8})$ also afforded closed and open conformers. The most stable structure of $K^+(\text{Asym1DB24C8})$, isomer **asym1-a** (Figure 6c), exhibited a closed conformation with benzene-benzene distance of 4.72 \AA . The second and third most stable structures of $K^+(\text{Asym1DB24C8})$, isomers **asym1-b** and **asym1-c** (not shown), also exhibited closed conformation. The calculated theoretical CCS of these three conformers was $\sim 166 \text{\AA}^2$. The fourth most stable structure, isomer **asym1-d** (Figure 6d)

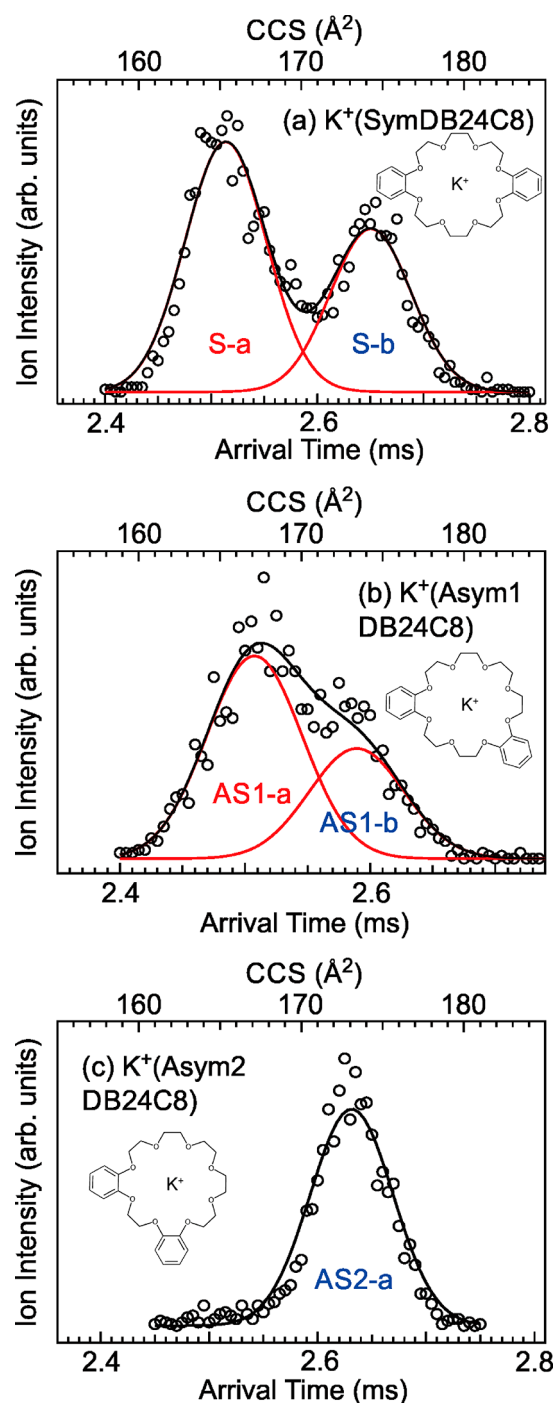


Figure 5. ATDs of (a) $K^+(\text{SymDB24C8})$, (b) $K^+(\text{Asym1DB24C8})$, and (c) $K^+(\text{Asym2DB24C8})$ (open circles). The ATD curves were reproduced employing Gaussian functions (red curves). The sum of the components is drawn by black curves. The pressure and temperature of the He buffer gas were (a) 0.491 ± 0.004 Torr and 85.95 ± 0.30 K, (b) 0.484 ± 0.004 Torr and 85.79 ± 0.67 K, and (c) 0.490 ± 0.001 Torr and 85.77 ± 0.07 K.

could be classified as an open conformer (the benzene–benzene distance was 9.05 \AA). The theoretical CCS of isomer **asym1-d** was 171.3 \AA^2 , which was larger than those of the closed ones ($\sim 166 \text{ \AA}^2$). Regarding $K^+(\text{Asym2DB24C8})$, the benzene–benzene distances of the stable conformers did not vary greatly. The most stable structure of $K^+(\text{Asym2DB24C8})$ is shown in Figure 6e (isomer **asym2-a**). The benzene–

Table 2. Experimental CCS Values (\AA^2) Determined by the IM–MS Experiments with He Gas at 86 K (${}^{\text{DT}}\text{CCS}_{\text{He},86}$)^a

complexes	experimental	theoretical	
	${}^{\text{DT}}\text{CCS}_{\text{He},86}$ (\AA^2)	CCS (\AA^2) (conformers)	Bz–Bz distance (\AA)
$K^+(\text{SymDB24C8})$	165.3 ± 0.4 (S-a)	163.5 ± 0.6 (sym-a)	3.82
	174.4 ± 0.5 (S-b)	172.8 ± 0.8 (sym-b)	9.33
$K^+(\text{Asym1DB24C8})$	167.0 ± 0.4 (AS1-a)	165.9 ± 0.8 (asym1-a)	4.72
	173.5 ± 0.6 (AS1-b)	171.3 ± 0.6 (asym1-d)	9.05
$K^+(\text{Asym2DB24C8})$	173.1 ± 0.3 (AS2-a)	171.1 ± 0.8 (asym2-a)	6.62

^aTheoretical CCS values (\AA^2) of the optimized structures calculated employing the MOBCAL program. Distance between the two benzene rings in the complexes (\AA).

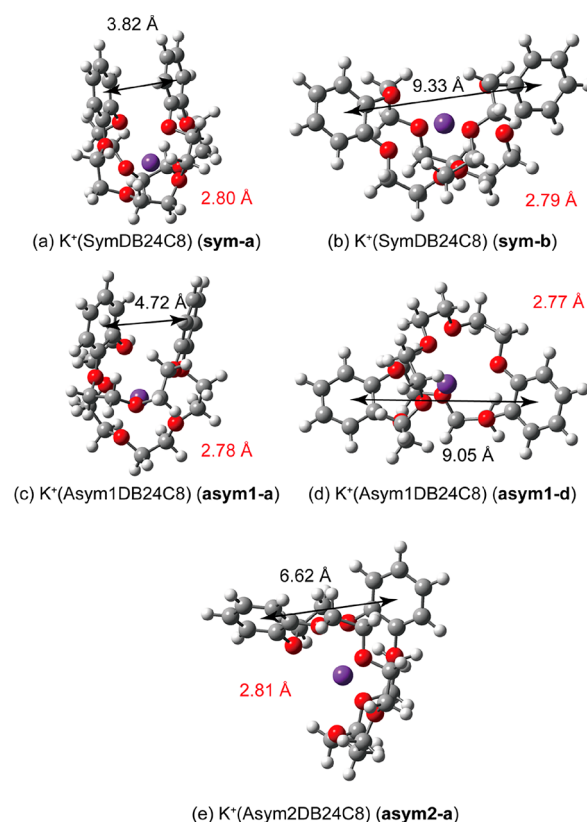


Figure 6. (a and b) Stable conformers of $K^+(\text{SymDB24C8})$. (c and d) Stable conformers of $K^+(\text{Asym1DB24C8})$. (e) Most stable conformer of $K^+(\text{Asym2DB24C8})$. Calculations were performed at the M05-2X/6-311++G(d,p) level. The numbers in black and red show the benzene–benzene distance and average distance between the K^+ ion and O atoms, respectively.

benzene distance and CCS were 6.62 \AA and 171.1 \AA^2 , respectively. These values were rather close to those of the open conformations of $K^+(\text{SymDB24C8})$ and $K^+(\text{Asym1DB24C8})$. Table 2 lists the experimental and theoretical values of CCS and the benzene–benzene distances of $K^+(\text{SymDB24C8})$, $K^+(\text{Asym1DB24C8})$, and $K^+(\text{Asym2DB24C8})$.

In the quantum chemical calculations of the complexes, we obtained many stable conformers other than those in Figure 6. Figure 7 displays the relative Gibbs energy of the stable

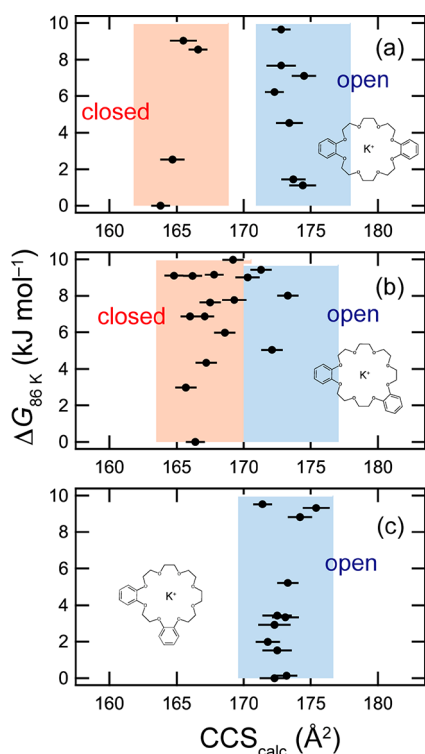


Figure 7. Calculated relative Gibbs energies of the stable conformers at 86 K ($\Delta G_{86\text{K}}$) against CCS of (a) $\text{K}^+(\text{SymDB24C8})$, (b) $\text{K}^+(\text{Asym1DB24C8})$, and (c) $\text{K}^+(\text{Asym2DB24C8})$. The red and blue regions indicated the observed CCS area drawn regarding the experimental ATD measurements in Figure 5.

conformers (up to 10 kJ mol^{-1}) at 86 K ($\Delta G_{86\text{K}}$) against their CCS values. The red and blue areas in Figure 7 were drawn based on the experimental CCS distribution with FWHM ($\sim 7 \text{ \AA}^2$; Figure 5). Regarding $\text{K}^+(\text{SymDB24C8})$, the stable conformers could be classified into two groups containing the calculated CCS values, ~ 166 and $\sim 174 \text{ \AA}^2$ (Figure 7a). All conformers were in the red or blue regions of Figure 7a. Thus, the two maxima observed at 165.3 and 174.4 \AA^2 of the experimental CCS curve (Figure 5a) were assigned to the closed and open conformer groups, respectively, although each of these conformers could not be separately detected. We also observed ATD of $\text{K}^+(\text{SymDB24C8})$ at 300 K (Figure S1, Supporting Information (SI)). The IM–MS experiment at 300 K could not detect the two components separately, and the CCS value experimentally determined at 300 K ($135.6 \pm 0.1 \text{ \AA}^2$) agrees well with the average value (135.1 \AA^2) of the stable conformers whose abundance ratios were determined by the Boltzmann distribution at 300 K.^{13,60} Hence, the interconversion between the open and closed conformers occurred at 300 K in $\text{K}^+(\text{SymDB24C8})$. Figure 7b shows the distribution of the stable conformers of $\text{K}^+(\text{Asym1DB24C8})$. The stable conformers were distributed much closer than in $\text{K}^+(\text{SymDB24C8})$. The separation of the two conformer groups was not as evident as in $\text{K}^+(\text{SymDB24C8})$ but these groups were still detected as two components on the experimental CCS curve (Figure 5b). Conversely, the CCS distribution of the stable conformers of $\text{K}^+(\text{Asym2DB24C8})$ was located only around $\sim 173 \text{ \AA}^2$ (Figure 7c). This coincided with the experimental ATD result that the ion signal was distributed only around 173.1 \AA^2 (Figure 5c).

As seen in Figures 5 and 7, CCS of $\text{K}^+(\text{DB24C8})$ strongly depended on the structural isomers or relative positions of the benzene rings. Previous reports suggested that larger crown ethers, such as 24-crown-8 and 30-crown-10, wrap around the metal ions to effectively hold the metal ions.⁴ Regarding $\text{K}^+(\text{SymDB24C8})$, this “wraparound” arrangement coincidentally resulted in the effective interaction between the benzene rings, thereby facilitating the formation of an intramolecular excimer upon UV excitation.⁴³ Hence, the positions of the benzene rings in DB24C8 affected both the sizes (the CCS values) of the complexes and their electronic structures. Benzocrown ethers assume planar forms of the O–C–C–O bond at the benzene rings,^{29,59,61} which strongly restricted the conformation of their crown rings. Regardless, the holding manner of K^+ ion by the 24C8 cavity was quite similar among $\text{K}^+(\text{SymDB24C8})$, $\text{K}^+(\text{Asym1DB24C8})$, and $\text{K}^+(\text{Asym2DB24C8})$, as shown in Figure 6. The crown ring of the 24C8 part wrapped the K^+ ion irrespective of the positions of the benzene rings in the 24C8 cavity. The estimated average distance between K^+ ion and the O atoms in the stable conformers was $\sim 2.80 \text{ \AA}$ for all of the stable conformers of $\text{K}^+(\text{SymDB24C8})$, $\text{K}^+(\text{Asym1DB24C8})$, and $\text{K}^+(\text{Asym2DB24C8})$. This also implied that the encapsulation processes of all of the $\text{K}^+(\text{DB24C8})$ complexes were similar. Hence, the difference in CCSs of $\text{K}^+(\text{SymDB24C8})$, $\text{K}^+(\text{Asym1DB24C8})$, and $\text{K}^+(\text{Asym2DB24C8})$ was not due to the encapsulation manner; it was mainly due to the difference in the benzene positions. Figure 8 shows the

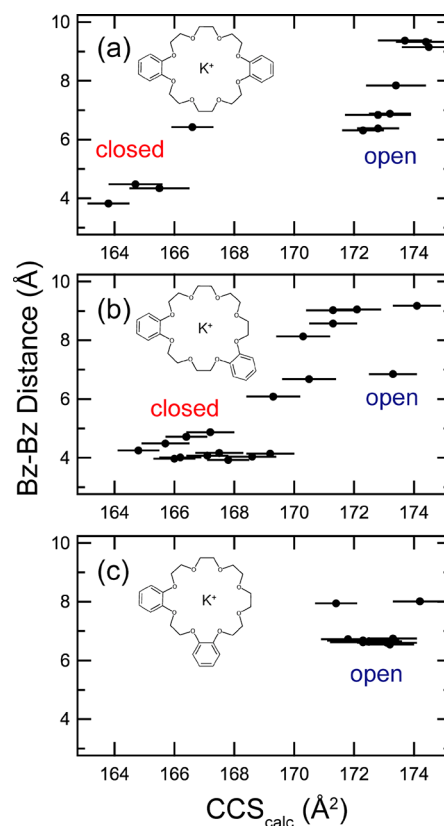


Figure 8. Distance between the benzene rings in the stable conformers against CCS for (a) $\text{K}^+(\text{SymDB24C8})$, (b) $\text{K}^+(\text{Asym1DB24C8})$, and (c) $\text{K}^+(\text{Asym2DB24C8})$. These figures were drawn for the stable conformers with the $\Delta G_{86\text{K}}$ of up to 10 kJ mol^{-1} .

benzene–benzene distance in the stable conformers of $K^+(DB24C8)$ against their CCS values. $K^+(SymDB24C8)$ exhibited a clear trend: the smaller the CCS values, the shorter the benzene–benzene distance. As aforementioned, the CCS difference between the closed and open conformers was not so clear in $K^+(Asym1DB24C8)$ as it was for $K^+(SymDB24C8)$, although a similar trend was observed between CCS and the benzene–benzene distance in $K^+(Asym1DB24C8)$ (Figure 8b). In $K^+(Asym2DB24C8)$, the distribution of CCS was narrower than that in $K^+(SymDB24C8)$ and $K^+(Asym1DB24C8)$ (Figure 8c). $K^+(Asym2DB24C8)$ did not feature large degrees of freedom in its conformation because of the narrowed distance between the benzene rings in the 24C8 cavity.

The spectroscopic results in Figures 3 and 4 availed some insights into the electronic and geometric structures of $K^+(DB24C8)$. The UVPD spectrum of $K^+(SymDB24C8)$ revealed broad features accompanied by weak, sharp bands.⁴³ The former and latter components in the spectrum were assigned to the closed and open conformers, respectively.⁴³ The broad features were attributed to the short lifetime of the excited state related to the formation of the intramolecular excimer,⁴³ which was confirmed in $K^+(SymDB24C8)$ by fluorescence spectroscopy in solution.⁴³ The coexistence of the closed and open conformers in the UVPD spectrum at ~ 10 K is consistent with the result of IM–MS that the open and closed conformers were separately detected at 86 K (Figure 5a). This IM–MS result implied that isomerization did not occur between the open and closed conformers in $K^+(SymDB24C8)$ at 86 or ~ 10 K. The intensity of the Gaussian components in the experimental ATDs directly represented the relative abundance ratio of the conformers. The experimental CCS data of $K^+(SymDB24C8)$ (Figure 5a) indicated that the abundance ratio between the closed and open conformers at 86 K was $\sim 1:0.65$ (S-a and S-b in Figure 5a). This ratio would probably be maintained even at ~ 10 K. The theoretical calculations predicted comparable transition probabilities for the electronic transitions of the closed and open conformers (Figure 1d of ref 43). Nevertheless, the band intensity of the open conformer was substantially weaker than that of the closed conformer in the UVPD spectrum. Therefore, this UVPD result for $K^+(SymDB24C8)$ suggested that the relative absorption intensity between the closed and open conformers was governed by the Franck–Condon factor (overlap of the vibrational wavefunctions of the electronic ground and excited states) and not by the relative abundance ratio.

In the UVPD spectrum of $K^+(Asym1DB24C8)$, broad and strong features are observed over the entire region of Figure 3b with a few weak, sharp bands. The IM–MS result (Figure 5b) implied that there was no interconversion between the closed and open conformers in $K^+(Asym1DB24C8)$ at 86 K and that the abundance ratio was $\sim 1:0.55$ between the closed and open conformers (AS1-a and AS1-b in Figure 5b) at 86 K. The theoretical calculations predicted that the number of closed conformers was substantially higher than that of the open ones (Figure 7b). Hence, the broad and sharp components in the UVPD spectrum of $K^+(Asym1DB24C8)$ were ascribed to the closed and open conformers. The fluorescence spectrum of $K^+(Asym1DB24C8)$ in solution (Figure 4b) did not exhibit significant Stokes-shifted fluorescence, indicating the absence of the intramolecular excimer in $K^+(Asym1DB24C8)$ upon UV excitation. Figure 9a shows the highest occupied molecular

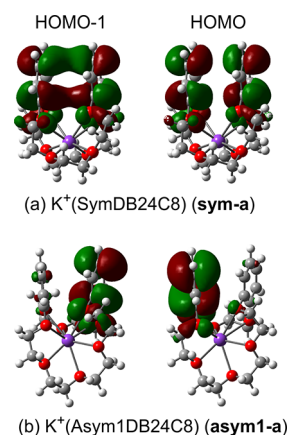


Figure 9. (a) HOMO and HOMO–1 of the most stable conformers of $K^+(SymDB24C8)$ (isomer **sym-a**) and (b) $K^+(Asym1DB24C8)$ (isomer **asym1-a**). The calculations were performed at the M05-2X/6-311++G(d,p) level.

orbital (HOMO) and second HOMO (HOMO–1) of the most stable conformer of $K^+(SymDB24C8)$ (isomer **sym-a**). The molecular orbitals (MOs) were equally delocalized in the two benzene rings of isomer **sym-a**.⁴³ This facilitated the formation of the excimer. Contrarily, MOs were mainly distributed in one of the benzene rings of the closed conformer of $K^+(Asym1DB24C8)$ (**asym1-a**, Figure 9b) because of nonequivalent situations in the two benzene rings: isomer **asym1-a** of $K^+(Asym1DB24C8)$ possessed a C_1 symmetry, whereas isomer **sym-a** of $K^+(SymDB24C8)$ was of the C_2 form. The distance between the two benzene rings was substantially longer in **asym1-a** (4.72 Å) than in **sym-a** (3.82 Å). This also prevented the formation of the intramolecular excimer in $K^+(Asym1DB24C8)$. Regarding $K^+(Asym2DB24C8)$, the distance between the benzene rings was rather large (>6 Å) and was unsuitable for the formation of the intramolecular excimer. The fluorescence spectrum of $K^+(Asym2DB24C8)$ did not prove the formation of the excimer (Figure 4c). These geometric features resulted in congested but sharp spectral features in the UVPD spectrum of $K^+(Asym2DB24C8)$.

CONCLUSION

As previously suggested, spectroscopic techniques, such as UVPD, demonstrate a high ability to separately detect different conformers.^{28,29,37,39} Since UV transition energy is highly sensitive to the conformation, UVPD spectroscopy performed under cold, gas-phase conditions could detect a minute difference in the conformation as a small difference in the UV transition energy. However, this spectroscopic technique is sometimes associated with the challenges of separating the conformers if they exhibit broad UV absorption due to the short lifetime of their excited states or spectroscopic congestion due to many degrees of vibrational freedom. This study demonstrated that the combination of UVPD spectroscopy and IM–MS was a powerful tool for resolving conformers and studying their electronic structures in host–guest chemistry. The conformations of the K^+ complexes of the three structural isomers of DB24C8, namely $K^+(SymDB24C8)$, $K^+(Asym1DB24C8)$, and $K^+(Asym2DB24C8)$, were investigated by UVPD spectroscopy, IM–MS in the gas phase, and fluorescence spectroscopy in methanol solutions. The IM–MS results at 86 K clearly revealed two components in $K^+(SymDB24C8)$ and

K⁺(Asym1DB24C8), which corresponded to the open and closed conformers. Further, the IM–MS experiment on K⁺(SymDB24C8) at 300 K could not separate the open and closed conformers because the interconversion between these conformers occurred at 300 K and not at 86 K. The UVPD spectrum of K⁺(Asym1DB24C8) at ~10 K exhibited broad features that were accompanied by sharp bands, indicating the coexistence of several isomers, and this agrees with the IM–MS result. K⁺(Asym2DB24C8) exhibited only a set of open conformations in the CCS experiment. The fluorescence spectra of these complexes in the methanol solution revealed that the intramolecular excimer was formed in K⁺(SymDB24C8) only. The crown cavity of DB24C8 wrapped around the K⁺ ion in K⁺(DB24C8), although the IM–MS results availed direct evidence of rapid cavity deformation and the reconstruction of stable conformers at 300 K. This study demonstrated that temperature-controlled IM–MS coupled with the introduction of bulky groups, such as aromatic rings to host molecules, could reveal the dynamic aspects of encapsulation in host–guest systems.

■ ASSOCIATED CONTENT

Supporting Information

The Supporting Information is available free of charge at <https://pubs.acs.org/doi/10.1021/acs.jpca.0c09068>.

Relative Gibbs energies, theoretical CCSs, benzene–benzene distances and the average distance between the K⁺ ion and O atoms of the stable conformers of K⁺(DB24C8) at 86 K, the observed and simulated ATDs of K⁺(SymDB24C8) at 300 K, the relative Gibbs energies and theoretical CCSs of the stable conformers of K⁺(SymDB24C8) at 300 K, geometrical coordinates of the conformers in Figure 6, and a full list of the authors of refs 12 and 55 (PDF)

■ AUTHOR INFORMATION

Corresponding Authors

Keiji Ohshimo – Department of Chemistry, Graduate School of Science, Tohoku University, Sendai 980-8578, Japan; orcid.org/0000-0002-2397-6896;
Email: keiji.ohshimo.d1@tohoku.ac.jp

Yoshiya Inokuchi – Department of Chemistry, Graduate School of Science, Hiroshima University, Higashi-Hiroshima 739-8526, Japan; orcid.org/0000-0001-7959-5315;
Email: y-inokuchi@hiroshima-u.ac.jp

Authors

Sota Tainaka – Department of Chemistry, Graduate School of Science, Tohoku University, Sendai 980-8578, Japan

Tomoyuki Ujihira – Department of Chemistry, Graduate School of Science, Hiroshima University, Higashi-Hiroshima 739-8526, Japan

Mayuko Kubo – Department of Chemistry, Graduate School of Science, Hiroshima University, Higashi-Hiroshima 739-8526, Japan

Motoki Kida – Department of Chemistry, Graduate School of Science, Hiroshima University, Higashi-Hiroshima 739-8526, Japan

Daisuke Shimoyama – Department of Chemistry, Graduate School of Science, Hiroshima University, Higashi-Hiroshima 739-8526, Japan

Satoru Muramatsu – Department of Chemistry, Graduate School of Science, Hiroshima University, Higashi-Hiroshima 739-8526, Japan; orcid.org/0000-0002-1575-7570

Manabu Abe – Department of Chemistry, Graduate School of Science, Hiroshima University, Higashi-Hiroshima 739-8526, Japan; orcid.org/0000-0002-2013-4394

Takeharu Haino – Department of Chemistry, Graduate School of Science, Hiroshima University, Higashi-Hiroshima 739-8526, Japan; orcid.org/0000-0002-0945-2893

Takayuki Ebata – Department of Chemistry, Graduate School of Science, Hiroshima University, Higashi-Hiroshima 739-8526, Japan; orcid.org/0000-0002-6236-9116

Fuminori Misaizu – Department of Chemistry, Graduate School of Science, Tohoku University, Sendai 980-8578, Japan; orcid.org/0000-0003-0822-6285

Complete contact information is available at:

<https://pubs.acs.org/10.1021/acs.jpca.0c09068>

Notes

The authors declare no competing financial interest.

■ ACKNOWLEDGMENTS

This work was supported by JSPS KAKENHI (Grant Nos. JP16H04098, JP20H00374 (Y.I.), and JP16K05641 (K.O.)), the Institute for Quantum Chemical Exploration, and The Salt Science Research Foundation (Grant No. 1916). Some of the calculations were conducted at the Research Center for Computational Science, Okazaki, Japan.

■ REFERENCES

- (1) Pedersen, C. J. Cyclic Polyethers and Their Complexes with Metal Salts. *J. Am. Chem. Soc.* **1967**, *89*, 7017–7036.
- (2) Pedersen, C. J. Cyclic Polyethers and Their Complexes with Metal Salts. *J. Am. Chem. Soc.* **1967**, *89*, 2495–2496.
- (3) Bright, D.; Truter, M. R. Crystal Structures of Complexes between Alkali-Metal Salts and Cyclic Polyethers. 1. Complex Formed between Rubidium Sodium Isothiocyanate and 2,3,11,12-Dibenzo-1,4,7,10,13,16-Hexaoxocyclo-Octadeca-2,11-Diene (Dibenzo-18-Crown-6). *J. Chem. Soc. B* **1970**, *0*, 1544–1550.
- (4) Bush, M. A.; Truter, M. R. Crystal-Structures of Complexes between Alkali-Metal Salts and Cyclic Polyethers. 4. Crystal-Structures of Dibenzo-30-Crown-10 (2,3-17,18-Dibenzo-1,4,7,10,13,16,19,22,25,28-Decaoxacyclotriaconta-2,17-Diene) and of Its Complex Potassium Iodide. *J. Chem. Soc., Perkin Trans. 2* **1972**, 345–350.
- (5) Bush, M. A.; Truter, M. R. Crystal Structures of Three Alkali-Metal Complexes with Cyclic Polyethers. *J. Chem. Soc. D* **1970**, 1439–1440.
- (6) Bush, M. A.; Truter, M. R. Crystal Structures of Complexes between Alkali-Metal Salts and Cyclic Polyethers. 2. Complex Formed from Sodium Bromide and 2,3,11,12-Dibenzo-1,4,7,10,13,16-Hexaoxocyclo-Octadeca-2,11-Diene ('Dibenzo-18-Crown-6'). *J. Chem. Soc. B* **1971**, *0*, 1440–1446.
- (7) Kanu, A. B.; Dwivedi, P.; Tam, M.; Matz, L.; Hill, H. H., Jr. Ion Mobility-Mass Spectrometry. *J. Mass Spectrom.* **2008**, *43*, 1–22.
- (8) Bowers, M. T. Ion Mobility Spectrometry: A Personal View of Its Development at UCSB. *Int. J. Mass Spectrom.* **2014**, *370*, 75–95.
- (9) Lanucara, F.; Holman, S. W.; Gray, C. J.; Evers, C. E. The Power of Ion Mobility-Mass Spectrometry for Structural Characterization and the Study of Conformational Dynamics. *Nat. Chem.* **2014**, *6*, 281–294.
- (10) Servage, K. A.; Silveira, J. A.; Fort, K. L.; Russell, D. H. Cryogenic Ion Mobility-Mass Spectrometry: Tracking Ion Structure from Solution to the Gas Phase. *Acc. Chem. Res.* **2016**, *49*, 1421–1428.

- (11) Clemmer, D. E.; Russell, D. H.; Williams, E. R. Characterizing the Conformation: toward a Structural Understanding of the Proteome. *Acc. Chem. Res.* **2017**, *50*, 556–560.
- (12) Gabelica, V.; Shvartsburg, A. A.; Afonso, C.; Barran, P.; Benesch, J. L. P.; Bleiholder, C.; Bowers, M. T.; Bilbao, A.; Bush, M. F.; Campbell, J. L.; et al. Recommendations for Reporting Ion Mobility Mass Spectrometry Measurements. *Mass Spectrom. Rev.* **2019**, *38*, 291–320.
- (13) Wyttenbach, T.; Pierson, N. A.; Clemmer, D. E.; Bowers, M. T. Ion Mobility Analysis of Molecular Dynamics. *Annu. Rev. Phys. Chem.* **2014**, *65*, 175–196.
- (14) Milloy, H. B.; Elford, M. T. Mass Discrimination in Ion Sampling from Drift Tubes. *Int. J. Mass Spectrom. Ion Phys.* **1975**, *18*, 21–31.
- (15) Johnsen, R.; Chen, A.; Biondi, M. A. Dissociative Charge Transfer of He⁺ Ions with H₂ and D₂ Molecules from 78 to 330 K. *J. Chem. Phys.* **1980**, *72*, 3085–3088.
- (16) Koizumi, T.; Kobayashi, N.; Kaneko, Y. Mobilities of Ne⁺ and Ar⁺ Ions in He Gas at 82 K. *J. Phys. Soc. Jpn.* **1980**, *48*, 1678–1682.
- (17) Misaizu, F.; Hori, N.; Tanaka, H.; Komatsu, K.; Furuya, A.; Ohno, K. Isomer-Selected Photoreactions of Gas-Phase Cluster Ions. *Eur. Phys. J. D* **2009**, *52*, 59–62.
- (18) von Helden, G.; Wyttenbach, T.; Bowers, M. T. Inclusion of a MALDI Ion Source in the Ion Chromatography Technique: Conformational Information on Polymer and Biomolecular Ions. *Int. J. Mass Spectrom. Ion Processes* **1995**, *146-147*, 349–364.
- (19) Wyttenbach, T.; Kemper, P. R.; Bowers, M. T. Design of a New Electrospray Ion Mobility Mass Spectrometer. *Int. J. Mass Spectrom.* **2001**, *212*, 13–23.
- (20) May, J. C.; Russell, D. H. A Mass-Selective Variable-Temperature Drift Tube Ion Mobility-Mass Spectrometer for Temperature Dependent Ion Mobility Studies. *J. Am. Soc. Mass Spectrom.* **2011**, *22*, 1134–1145.
- (21) Ujma, J.; Giles, K.; Morris, M.; Barran, P. E. New High Resolution Ion Mobility Mass Spectrometer Capable of Measurements of Collision Cross Sections from 150 to 520 K. *Anal. Chem.* **2016**, *88*, 9469–9478.
- (22) Ohshimo, K.; Sato, R.; Misaizu, F. Intramolecular Dispersion Attraction in Tetraalkylammonium Cations Revealed by Cryogenic Ion Mobility Mass Spectrometry. *J. Phys. Chem. A* **2020**, *124*, 7999–8004.
- (23) Weis, P.; Bierweiler, T.; Vollmer, E.; Kappes, M. M. Au₉⁺: Rapid Isomerization Reactions at 140 K. *J. Chem. Phys.* **2002**, *117*, 9293–9297.
- (24) Ohshimo, K.; Miyazaki, S.; Hattori, K.; Misaizu, F. Long-Distance Proton Transfer Induced by a Single Ammonia Molecule: Ion Mobility Mass Spectrometry of Protonated Benzocaine Reacted with NH₃. *Phys. Chem. Chem. Phys.* **2020**, *22*, 8164–8170.
- (25) Lee, S.; Wyttenbach, T.; Vonhelden, G.; Bowers, M. T. Gas-Phase Conformations of Li⁺, Na⁺, K⁺, and Cs⁺ Complexed with 18-Crown-6. *J. Am. Chem. Soc.* **1995**, *117*, 10159–10160.
- (26) Dearden, D. V.; Ferrell, T. A.; Asplund, M. C.; Zilch, L. W.; Julian, R. R.; Jarrold, M. F. One Ring to Bind Them All: Shape-Selective Complexation of Phenylenediamine Isomers with Cucurbit[6]Urils in the Gas Phase. *J. Phys. Chem. A* **2009**, *113*, 989–997.
- (27) Zhang, H.; Grabenauer, M.; Bowers, M. T.; Dearden, D. V. Supramolecular Modification of Ion Chemistry: Modulation of Peptide Charge State and Dissociation Behavior through Complexation with Cucurbit[*n*]Urils (*n* = 5, 6) or 5-Cyclodextrin. *J. Phys. Chem. A* **2009**, *113*, 1508–1517.
- (28) Inokuchi, Y.; Boyarkin, O. V.; Kusaka, R.; Haino, T.; Ebata, T.; Rizzo, T. R. UV and IR Spectroscopic Studies of Cold Alkali Metal Ion-Crown Ether Complexes in the Gas Phase. *J. Am. Chem. Soc.* **2011**, *133*, 12256–12263.
- (29) Inokuchi, Y.; Boyarkin, O. V.; Kusaka, R.; Haino, T.; Ebata, T.; Rizzo, T. R. Ion Selectivity of Crown Ethers Investigated by UV and IR Spectroscopy in a Cold Ion Trap. *J. Phys. Chem. A* **2012**, *116*, 4057–4068.
- (30) Rodriguez, J. D.; Lisy, J. M. Infrared Spectroscopy of Gas-Phase Hydrated K⁺:18-Crown-6 Complexes: Evidence for High Energy Conformer Trapping Using the Argon Tagging Method. *Int. J. Mass Spectrom.* **2009**, *283*, 135–139.
- (31) Hurtado, P.; Hortal, A. R.; Gámez, F.; Hamad, S.; Martínez-Haya, B. Gas-Phase Complexes of Cyclic and Linear Polyethers with Alkali Cations. *Phys. Chem. Chem. Phys.* **2010**, *12*, 13752–13758.
- (32) Cooper, T. E.; Carl, D. R.; Oomens, J.; Steill, J. D.; Armentrout, P. B. Infrared Spectroscopy of Divalent Zinc and Cadmium Crown Ether Systems. *J. Phys. Chem. A* **2011**, *115*, 5408–5422.
- (33) Gamez, F.; Hurtado, P.; Martínez-Haya, B.; Berden, G.; Oomens, J. Vibrational Study of Isolated 18-Crown-6 Ether Complexes with Alkaline-Earth Metal Cations. *Int. J. Mass Spectrom.* **2011**, *308*, 217–224.
- (34) Kim, H. J.; Shin, W. J.; Choi, C. M.; Lee, J. H.; Kim, N. J. Electronic Photodepletion Spectroscopy of Dibenzo-18-Crown-6 with a Potassium Ion. *Bull. Korean Chem. Soc.* **2008**, *29*, 1973–1976.
- (35) Choi, C. M.; Kim, H. J.; Lee, J. H.; Shin, W. J.; Yoon, T. O.; Kim, N. J.; Heo, J. Ultraviolet Photodepletion Spectroscopy of Dibenzo-18-Crown-6-Ether Complexes with Alkali Metal Cations. *J. Phys. Chem. A* **2009**, *113*, 8343–8350.
- (36) Choi, C. M.; Lee, J. H.; Choi, Y. H.; Kim, H. J.; Kim, N. J.; Heo, J. Ultraviolet Photodepletion Spectroscopy of Dibenzo-18-Crown-6-Ether Complexes with Alkaline Earth Metal Divalent Cations. *J. Phys. Chem. A* **2010**, *114*, 11167–11174.
- (37) Choi, C. M.; Choi, D. H.; Heo, J.; Kim, N. J.; Kim, S. K. Ultraviolet-Ultraviolet Hole Burning Spectroscopy in a Quadrupole Ion Trap: Dibenzo[18]Crown-6 Complexes with Alkali Metal Cations. *Angew. Chem., Int. Ed.* **2012**, *51*, 7297–7300.
- (38) Choi, C. M.; Baek, J. Y.; Park, K. S.; Heo, J.; Kim, N. J. Conformation-Specific Ultraviolet Spectroscopy of Benzo-18-Crown-6 Complexes with a Potassium Cation. *Chem. Phys. Lett.* **2014**, *593*, 150–153.
- (39) Inokuchi, Y.; Soga, K.; Hirai, K.; Kida, M.; Morishima, F.; Ebata, T. Ultraviolet Photodissociation Spectroscopy of the Cold K⁺Calix[4]Arene Complex in the Gas Phase. *J. Phys. Chem. A* **2015**, *119*, 8512–8518.
- (40) Inokuchi, Y.; Ebata, T.; Rizzo, T. R.; Boyarkin, O. V. Microhydration Effects on the Encapsulation of Potassium Ion by Dibenzo-18-Crown-6. *J. Am. Chem. Soc.* **2014**, *136*, 1815–1824.
- (41) Inokuchi, Y.; Nakatsuma, M.; Kida, M.; Ebata, T. Conformation of Alkali Metal Ion-Benzo-12-Crown-4 Complexes Investigated by UV Photodissociation and UV-UV Hole-Burning Spectroscopy. *J. Phys. Chem. A* **2016**, *120*, 6394–6401.
- (42) Inokuchi, Y.; Kida, M.; Ebata, T. Geometric and Electronic Structures of Dibenzo-15-Crown-5 Complexes with Alkali Metal Ions Studied by UV Photodissociation and UV-UV Hole-Burning Spectroscopy. *J. Phys. Chem. A* **2017**, *121*, 954–962.
- (43) Kida, M.; Kubo, M.; Ujihira, T.; Ebata, T.; Abe, M.; Inokuchi, Y. Selective Probing of Potassium Ion in Solution by Intramolecular Excimer Fluorescence of Dibenzo-Crown Ethers. *ChemPhysChem* **2018**, *19*, 1331–1335.
- (44) Papadopoulos, G.; Svendsen, A.; Boyarkin, O. V.; Rizzo, T. R. Spectroscopy of Mobility-Selected Biomolecular Ions. *Faraday Discuss.* **2011**, *150*, 243–255.
- (45) Papadopoulos, G.; Svendsen, A.; Boyarkin, O. V.; Rizzo, T. R. Conformational Distribution of Bradykinin Bk²⁺ H (2+) Revealed by Cold Ion Spectroscopy Coupled with FAIMS. *J. Am. Soc. Mass Spectrom.* **2012**, *23*, 1173–1181.
- (46) Kang, H.; Féraud, G.; Dedonder-Lardeux, C.; Jouvet, C. New Method for Double-Resonance Spectroscopy in a Cold Quadrupole Ion Trap and Its Application to UV-UV Hole-Burning Spectroscopy of Protonated Adenine Dimer. *J. Phys. Chem. Lett.* **2014**, *5*, 2760–2764.
- (47) Kobayashi, Y.; Inokuchi, Y.; Ebata, T. Ion Core Structure in (CS₂)_{*n*}⁺ and (CS₂)_{*n*}⁻ (*n* = 3–10) Studied by Infrared Photodissociation Spectroscopy. *J. Chem. Phys.* **2008**, *128*, 164319.

(48) Kelly, R. T.; Tolmachev, A. V.; Page, J. S.; Tang, K.; Smith, R. D. The Ion Funnel: Theory, Implementations, and Applications. *Mass Spectrom. Rev.* **2009**, *29*, 294–312.

(49) May, J. C.; Russell, D. H. A Mass-Selective Variable-Temperature Drift Tube Ion Mobility-Mass Spectrometer for Temperature Dependent Ion Mobility Studies. *J. Am. Soc. Mass Spectrom.* **2011**, *22*, 1134–1145.

(50) Matsuo, Y.; Okada, H.; Ueno, H. *Endohedral Lithium-Containing Fullerenes: Preparation, Derivatization, and Application*; Springer Nature: Singapore, 2017.

(51) Goto, H.; Osawa, E. Corner Flapping: A Simple and Fast Algorithm for Exhaustive Generation of Ring Conformations. *J. Am. Chem. Soc.* **1989**, *111*, 8950–8951.

(52) Goto, H.; Osawa, E. An Efficient Algorithm for Searching Low-Energy Conformers of Cyclic and Acyclic Molecules. *J. Chem. Soc., Perkin Trans. 2* **1993**, 187–198.

(53) Inokuchi, Y.; Ebata, T.; Rizzo, T. R. Solvent Effects on the Encapsulation of Divalent Ions by Benzo-18-Crown-6 and Benzo-15-Crown-5. *J. Phys. Chem. A* **2015**, *119*, 8097–8105.

(54) Inokuchi, Y.; Ebata, T.; Ikeda, T.; Haino, T.; Kimura, T.; Guo, H.; Furutani, Y. New Insights into Metal Ion-Crown Ether Complexes Revealed by SEIRA Spectroscopy. *New J. Chem.* **2015**, *39*, 8673–8680.

(55) Frisch, M. J.; et al. *Gaussian 09*, revision A.02; Gaussian, Inc.: Wallingford, CT, 2009.

(56) Mesleh, M. F.; Hunter, J. M.; Shvartsburg, A. A.; Schatz, G. C.; Jarrold, M. F. Structural Information from Ion Mobility Measurements: Effects of the Long-Range Potential. *J. Phys. Chem.* **1996**, *100*, 16082–16086.

(57) Campuzano, I.; Bush, M. F.; Robinson, C. V.; Beaumont, C.; Richardson, K.; Kim, H.; Kim, H. I. Structural Characterization of Drug-Like Compounds by Ion Mobility Mass Spectrometry: Comparison of Theoretical and Experimentally Derived Nitrogen Collision Cross Sections. *Anal. Chem.* **2012**, *84*, 1026–1033.

(58) Wingfield, J. N. The Synthesis and Complexation of Two 24-Crown-8 Cyclic Polyethers. *Inorg. Chim. Acta* **1980**, *45*, L157–L159.

(59) Kokubu, S.; Kusaka, R.; Inokuchi, Y.; Haino, T.; Ebata, T. Laser Spectroscopic Study on (Dibenzo-24-Crown-8-Ether)-Water and -Methanol Complexes in Supersonic Jets. *Phys. Chem. Chem. Phys.* **2010**, *12*, 3559–3565.

(60) Gidden, J.; Bowers, M. T. Gas-Phase Conformational and Energetic Properties of Deprotonated Dinucleotides. *Eur. Phys. J. D* **2002**, *20*, 409–419.

(61) Kusaka, R.; Inokuchi, Y.; Ebata, T. Structure of Hydrated Clusters of Dibenzo-18-Crown-6-Ether in a Supersonic Jet-Encapsulation of Water Molecules in the Crown Cavity. *Phys. Chem. Chem. Phys.* **2008**, *10*, 6238–6244.